$Au_{279}(SR)_{84}$: The Smallest Gold Thiolate Nanocrystal That Is Metallic and the Birth of Plasmon

Naga Arjun Sakthivel,[†] Mauro Stener,[‖] Luca Sementa,[§] Alessandro Fortunelli,[*,§] Guda Ramakrishna,[*,‡] and Amala Dass[*,†]

[†]Department of Chemistry and Biochemistry, University of Mississippi, Oxford, Mississippi 38677, United States
[‡]Department of Chemistry, Western Michigan University, Kalamazoo, Michigan 49008, United States
[‖]Dipartimento di Scienze Chimiche e Farmaceutiche, Università di Trieste, Trieste I-34127, Italy
[§]CNR-ICCOM & IPCF, Consiglio Nazionale delle Ricerche, Pisa I-56124, Italy

Supporting Information

ABSTRACT: We report a detailed study on the optical properties of $Au_{279}(SR)_{84}$ using steady-state and transient absorption measurements to probe its metallic nature, time-dependent density functional theory (TDDFT) studies to correlate the optical spectra, and density of states (DOS) to reveal the factors governing the origin of the collective surface plasmon resonance (SPR) oscillation. Au_{279} is the smallest identified gold nanocrystal to exhibit SPR. Its optical absorption exhibits SPR at 510 nm. Power-dependent bleach recovery kinetics of Au_{279} suggests that electron dynamics dominates its relaxation and it can support plasmon oscillations. Interestingly, TDDFT and DOS studies with different tail group residues ($-CH_3$ and $-Ph$) revealed the important role played by the tail groups of ligands in collective oscillation. Also, steady-state and time-resolved absorption for Au_{36}, Au_{44}, and Au_{133} were studied to reveal the *molecule-to-metal* evolution of aromatic AuNMs. The optical gap and transient decay lifetimes decrease as the size increases.

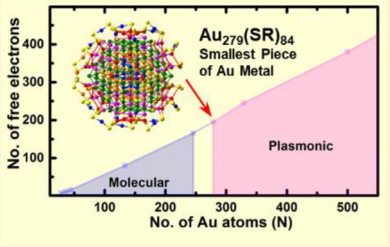

Over the last two decades, the phenomenon of surface plasmon resonance (SPR) has gained prime attention, and major advances have been made toward targeted cancer therapy,[1,2] catalysis,[3] and energy devices.[4] Among the colloidal metal particles, gold nanoparticles have attracted attraction since ancient times for their aesthetics and exquisite optical properties. The optical properties of these nanoparticles vary significantly from the bulk gold and with size and type of passivating agent employed because of quantum confinement effect.[5−7] The size and structure of the nanoparticle have been understood to be the major factors influencing the evolution of surface plasmon resonance (SPR) and its intensity.[8,9] Optical response of the nanoparticles can be tuned by understanding their dependence on numerous factors, e.g., the intensity of the SPR increases as the size increases, and by alloying with a heteroatom.[10−13]

The seminal work of Whetten et al. on gold nanomolecules (AuNMs) single out an approximate boundary for the core size at which the molecular-to-metallic evolution occurs.[5] More detailed investigations have then followed on the emergence of plasmonic response in AuNMs and have further specified the size range between 200 and 400 Au atoms as the range in which incipient plasmonic features appear.[14,15] However, the *precise size at which the evolution takes place and the details of this evolution are still unclear to date.*

Among different techniques, time-resolved transient absorption measurements were often used to differentiate molecule-like and plasmon-like transitions in AuNMs. Metal nanocrystals that are plasmonic show prominent bleach near 530 nm and exhibit power-dependent decay of the transients that can be modeled with a two-temperature model.[16,17] On the other hand, molecule-like nanoparticles show single-particle transitions with interesting excited-state absorption characteristics and power-independent transient decay traces.[18−25] In this study, ultrafast transient absorption measurements were carried out to clarify molecule-like versus plasmon-like transitions of 4-*tert*-butylbenzenethiolate (TBBT)-protected AuNMs.

Since Faraday's work[26] on minute metal particles, theoretical models such as Mie theory, Drude model, jellium model, etc. have been applied to correlate the experimental optical behavior of nanoparticles depending on their size, atomic structure, electronic structure, properties of the nanoparticle environment, etc.[8,27−30] It should be stressed that the surface plasmon resonance is a collective phenomenon and therefore cannot be described by a single-particle model, as it entails the coupling of many excited configurations. Several investigations have shown that a convenient method that is able to describe both collective and molecular-type single-electron independent excitations and is also computationally affordable for systems up to 1−2 thousand atoms is time-dependent density functional theory (TDDFT), and this method has been widely applied to investigate the optical response of metal NMs.[31]

Accepted: February 26, 2018

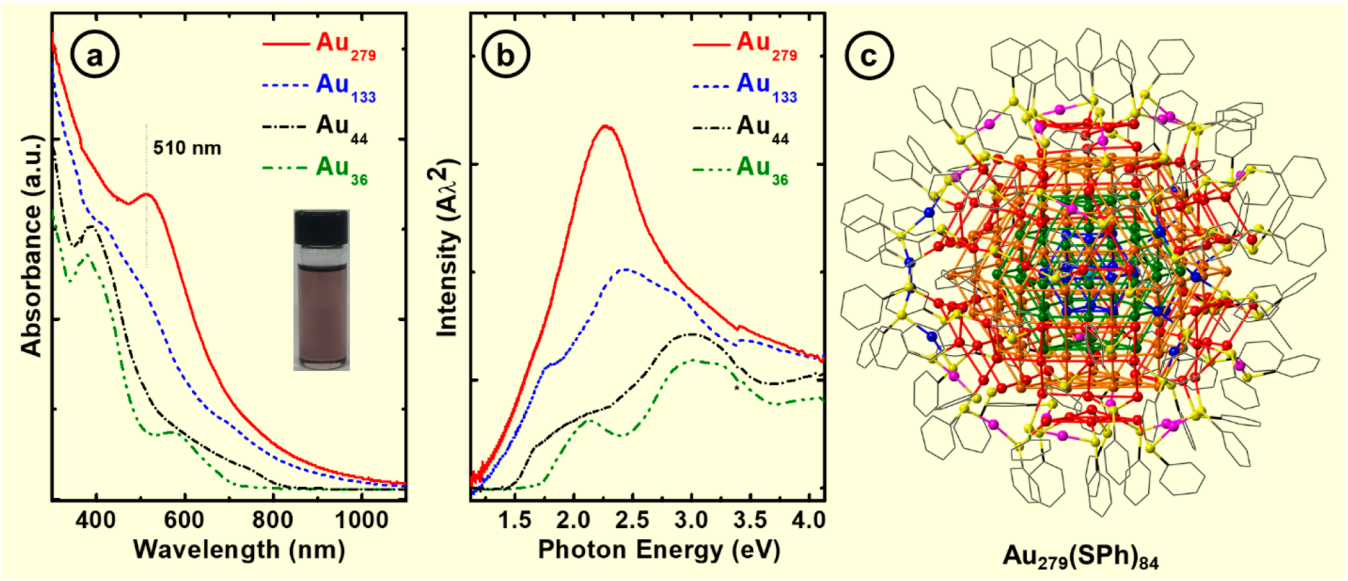

Figure 1. (a) UV−vis−NIR absorption spectra and (b) photon energy plot of Au_{279} TBBT-protected gold nanocrystals (red, solid) compared with $Au_{36}(SR)_{24}$ (olive green, dash−dot−dot), $Au_{44}(SR)_{28}$ (black, dash−dot), and $Au_{133}(SR)_{52}$ (blue, dash) (SR = TBBT). The asterisk indicates the instrumental artifact due to detector/source changeover. (c) $Au_{279}(SPh)_{84}$ structure: X-ray model of $Au_{279}S_{84}$ with Ph residues added in the model for computational purposes. Au_{249} core−shell: cyan, center Au atom; blue, Au_{12} cuboctahedral (CO) shell; green, Au_{42} CO shell; orange, Au_{92} CO shell; and red, Au_{102} shell. Ligand shell: yellow, sulfur; magenta, monomeric Au; blue, dimeric Au; and black wire, carbon (hydrogen atoms of Ph group are excluded for clarity).

Numerous experimental and computational works have been performed to reveal the molecule-to-metal transitions and structure dependence with size.[24,25,32−35]

To date, alkanethiolate series[10−12,15] of AuNMs [$Au_{25}(SR)_{18}$, $Au_{38}(SR)_{24}$, ... $Au_{144}(SR)_{60}$, $Au_{329}(SR)_{84}$, $Au_{\sim500}(SR)_{\sim120}$, and $Au_{\sim940}(SR)_{\sim160}$ (R is alkyl chain or phenylethane group)] have been widely studied to probe the evolution of molecular-to-metallic behavior (Table S1).[5,6,24,25] However, only $Au_{25}(SR)_{18}$ and $Au_{38}(SR)_{24}$ structures have been crystallographically resolved.[36−39] The lack of crystallographic structures of plasmonic gold nanocrystals has been hampering the understanding of the role of ligands in collective oscillation and the origin of SPR.

Recent advancements employing the bulky and rigid TBBT[40] as a ligand to favor the crystal growth has rendered the crystal structure determination of Faradaurate-279 (F-279, $Au_{279}(SPh\text{-}tBu)_{84}$) nanocrystal[41] feasible. TBBT-protected series of AuNMs[40−47] include $Au_{28}(SR)_{20}$, $Au_{36}(SR)_{24}$, $Au_{44}(SR)_{28}$, $Au_{52}(SR)_{32}$, $Au_{92}(SR)_{44}$, $Au_{133}(SR)_{52}$, and $Au_{279}(SR)_{84}$ [SR, TBBT]. Au_{36}, Au_{133}, and Au_{279} are thermochemically stable and can be synthesized in high yields, whereas others are not as stable and are not readily synthesizable. Also, no stable intermediate size has been identified between Au_{133} and Au_{279} (Figure S1). Thus, the three stable AuNMs (36, 1.3 nm; 133, 1.7 nm; and 279, 2.2 nm) were chosen for the optical and transient absorption measurements (Table S1 lists various stable sizes in three AuNMs series). Additionally, Au_{44} (1.4 nm) was studied to better illustrate the transition from molecular-like to metal-like behavior in TBBT series. Zhou et al. have recently reported the excited-state dynamics of Au_{28}, Au_{36}, Au_{44}, and Au_{52} periodic face-centered cubic NMs.[48]

F-279 is a critical size in the transition from molecule to metal in AuNMs with a core size of 2.2 nm. $Au_{246}(S{-}C_6H_4{-}CH_3)_{80}$ has a core-size of 2.2 nm as well, but it is molecule-like with absorption features at 400, 470, and 600 nm,[49,50] even though the difference between $Au_{246}(SR)_{80}$ and $Au_{279}(SR)_{84}$ is only 33 Au and 4 ligands. Other gold nanocrystal sizes larger than F-279 are all plasmonic: F-329 (core, 2.2 nm), F-500 (2.4 nm), and F-940 (3 nm).[10−12,51] Distinct types of ligands (aliphatic, aromatic, and bulky) produce discrete stable sizes in the molecule-to-metal regime. There are no AuNMs series that have been reported which span the whole molecule-to-metal transition in small increments (...1.9, 2.0, 2.1, 2.2, 2.3 nm, etc.). Can the stable sizes across various ligand-protected series of AuNMs be compared to determine where the molecule-to-metal transition occurs precisely? Does the contribution from ligand group to the properties of AuNMs makes it nonlinear to draw a comparison? Although the electronic features of the ligands play a vital role in the optical properties of AuNMs, the cross comparison of the different series of AuNMs is the only conceivable way to underpin the precise point of molecule-to-metal transition. While $Au_{144}(SR)_{60}$ is the smallest known AuNM to exhibit characteristics of metallic behavior in the form of *core-localized plasmon resonance* (CLPR),[21] among the three equally sized 2.2 nm nanomolecules (Au_{246}, Au_{279}, and Au_{329}), F-279 is the smallest gold thiolate nanocrystal to exhibit *classical SPR* with a strong absorption band at 510 nm. Therefore, F-279 is *the smallest identified piece of Au metal*. The next question that might arise is, could there be a stable intermediate size between $Au_{246}(SR)_{80}$ and $Au_{279}(SR)_{84}$ which is metallic? This is one of the next important open questions to be addressed in this field of research. Xu et al. have predicted that the evolution from molecule-to-metal transition in AuNMs might occur at ∼263 Au atoms by interpolating the trend between band gap and number of Au atoms for known NMs.[52]

Herein, we report the optical properties of F-279 and the evolution of molecular to metal-like behavior in aromatic thiolate-protected AuNMs for the first time, using (a) optical absorption, (b) computational studies on optical spectra of F-279 compared with Au_{133}, (c) projected density of states (PDOS) of F-279 structure with $-CH_3$ and $-C_6H_5$ residues, and (d) transient absorption measurements.

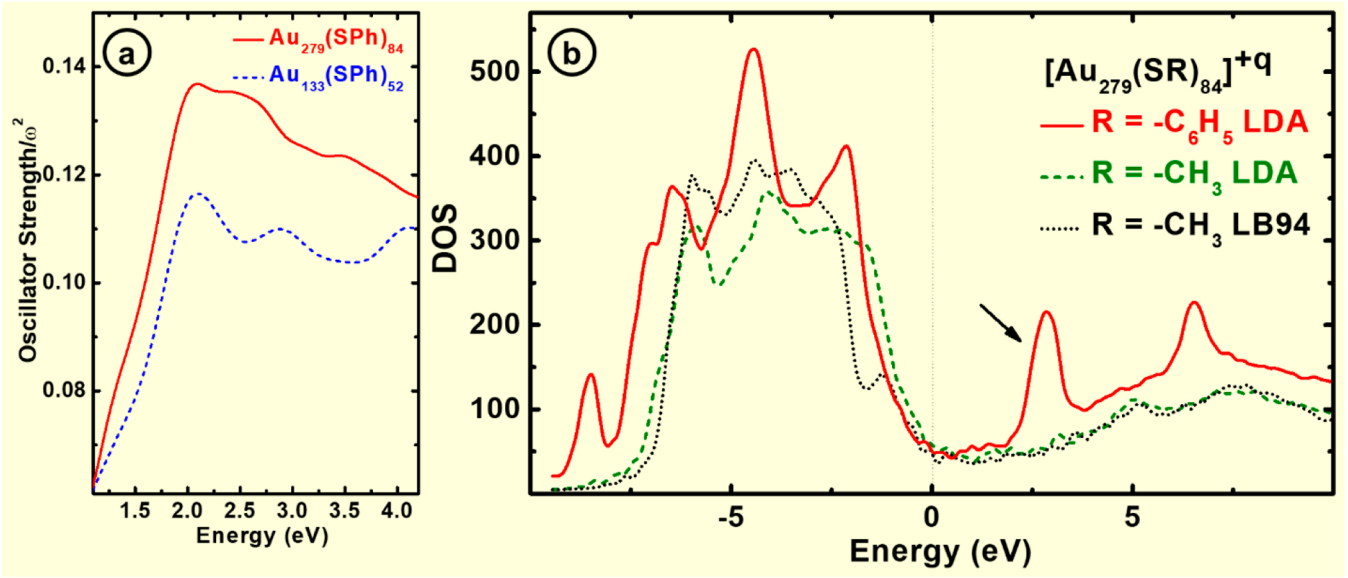

Figure 2. (a) Simulated photon energy plots of $Au_{133}(SPh)_{52}$ and $Au_{279}(SPh)_{84}$ using a RT-TDDFT/PBE approach (see the text for more details). (b) Total DOS of $[Au_{279}(SR)_{84}]^{+q}$ systems with two different ligands (R) and xc-functionals (q = +1 for LDA, q = +3 for LB94) with the zero of energy set at the Fermi energy.

The optical absorption spectra of $Au_{279}(SR)_{84}$ compared with $Au_{36}(SR)_{24}$, $Au_{44}(SR)_{28}$, and $Au_{133}(SR)_{52}$ TBBT-protected series of AuNMs are shown in Figure 1a. The Au_{36}, Au_{44}, and Au_{133} have unique optical absorption features for discrete transitions indicative of molecule-like behavior. Au_{36} has two absorption features at 375 and 575 nm and a broad shoulder around 410 nm. Au_{44} has a prominent feature at 380 nm and a broad absorption band near 750 nm. Au_{133} has a broad, strong absorption feature at 510 nm and minor features at 430 and 710 nm. The F-279 nanocrystals exhibit plasmonic behavior with SPR band centered at 510 nm. Interestingly, the SPR band is red-shifted compared to F-329, which is located at 495 nm.[10] Such a red shift is imparted by the aromatic ligand.[53]

The size-dependent optical spectra in Figure 1 are reminiscent of the report by Whetten et al. on a series of alkanethiolate-protected AuNMs.[5] That is, as the size decreases to <2 nm, the plasmonic feature diminishes and transforms into molecular-like transitions. The features are unique to each NM sizes because of the quantum confinement effect. The onset of electronic transitions from highest occupied levels (HOMOs) to the lowest unoccupied molecular orbitals (LUMOs) in alkanethiolate-protected AuNMs were observed at ~1.6 eV, and it remains nearly the same throughout the evolution from molecular to plasmonic behavior. However, in the case of aromatic TBBT-protected series of AuNMs, the onset of electronic transitions varies across the distinct sizes, i.e., onset energy decreases as the size increases: Au_{36}, ~1.7 eV and Au_{44}, ~ 1.5 eV (Figure 1b). The SPR band of F-279 is centered at 2.25 eV. The 510 nm feature of Au_{133} is reminiscent of emergent SPR, which can be readily seen in the photon energy plot at the 2.45 eV feature (Figure 1b). Figure 1c reports the $Au_{279}(SPh)_{84}$ structure by theoretical addition of Ph residues to the $Au_{279}S_{84}$ experimental crystallographic structure (see the Supporting Information for details).

Figure 2a reports the simulated TDDFT spectrum of $Au_{279}(SPh)_{84}$ and compares it with the previously reported simulated spectrum of $Au_{133}(SPh)_{52}$,[40] both obtained using the Perdew–Burke–Ernzerhof (PBE) xc-functional. An inspection of this figure immediately conveys that the absorption intensity between 460 and 600 nm increases significantly in the 2–4 eV region for the larger species: the nearly flat profile of the $Au_{133}(SPh)_{52}$ spectrum clearly transforms into a well-pronounced, although somewhat broad peak in $Au_{279}(SPh)_{84}$. Considering the limitations associated with a TDDFT approach using a PBE xc-functional (which lacks Hartree–Fock exchange and Coulombic-tail terms in the potential[54]), particularly in the RT-TDDFT formalism that is known to overestimate s/d damping of the optical response in AuNMs,[55] the present simulations confirm the *birth of the plasmon resonance* in TBBT-protected Au nanocrystals and thus the soundness of the experimental analysis. A further question in this respect is how much of this enhanced optical response is due to a classical free-electron plasmonic phenomenon or to a resonance effect of the Au–S core with the aromatic thus conjugated –SPh ligands, as discussed in ref 56. Previous detailed investigations on the emergence of plasmonic response in $Au_n(SR)_m$ NMs[14,15] suggest in fact that $Au_{279}(SR)_{84}$ should be right on the verge of a classical plasmonic behavior and thus exhibit an absorption peak in the ~530 nm region a bit less well-defined than that shown in Figure 2. A DOS analysis provides insight into this question. As shown in Figure 2b via a comparison between the $Au_{279}(SPh)_{84}$ and $Au_{279}(SCH_3)_{84}$ total DOS at the LDA level (see also Figure S2 for more details and the PDOS projected onto the different atomic species), the presence of the aromatic ligands introduces peaks in the region of virtual orbitals close to the band gap that resonate with the Au–S core and distort and red-shift the DOS in the region of the occupied orbitals, an effect that contributes to the experimentally observed plasmonic enhancement in $Au_{279}(SPh\text{-}tBu)_{84}$.

To complete the theoretical analysis, in Figure S3 we report the simulated TDDFT spectra of $Au_{279}(SPh)_{84}$, $Au_{279}(SCH_3)_{84}$, $Au_{133}(SPh)_{52}$, and $Au_{133}(SCH_3)_{52}$, obtained using a different xc-functional, namely, the VS98 one,[57,58] which has been shown to provide a better description of plasmonic effects.[59] Unfortunately, because of computational limitations we can report only the TDDFT spectra calculated along the z-Cartesian component of the electric field, but they are sufficient to confirm and support on stronger grounds our previous analysis

and conclusions about the insurgence of a plasmon resonance in $Au_{279}(SPh)_{84}$ and the importance of ligand conjugation effects.

Time-resolved transient absorption spectroscopy is one technique that is best suited to probe molecule-to-metal transitions in AuNMs.[16−22] In the molecule-like regime, the NMs are described by single-particle excitations, while in the metallic regime, they show collective oscillations described by surface plasmon bleach.[16,17] Pump-power-dependent transient absorption measurements can differentiate molecule-like versus metal-like transitions. To unravel the evolution of molecule−metal transitions for the investigated AuNMs, transient absorption measurements were carried out after excitation at 370 nm, and corresponding excited-state absorption spectra at representative time delays for Au_{36}, Au_{44}, Au_{133}, and Au_{279} are presented in Figure 3. Transient species living much longer than 1 ns were observed for both Au_{36} and Au_{44} NMs, while the transients of Au_{133} decayed quickly, suggesting faster excited-state deactivation; interesting plasmon bleach features were observed for Au_{279}. Detailed femtosecond−nanosecond transient absorption measurements of Au_{36} (Figure S4) and Au_{44} (Figure S5) have shown excited-state recombination time constants of 115 ± 10 and 70 ± 8 ns, respectively. On the other hand, interesting excited-state absorption features were observed for Au_{133} (Figure S6) with a bleach at 500 nm and two positive excited-state absorption (ESA) spectra with maxima at 570 and 650 nm. However, all the transients of Au_{133} decayed very fast, and an average lifetime of 4.5 ps was determined from the analysis. The observed transient spectra for Au_{133} matched with what was reported earlier.[22] Interestingly, prominent bleach with a maximum at 540 nm and positive ESA around the bleach were observed for Au_{279} immediately after excitation and decays fast with increasing time delays (Figure S7). The observed transient spectral features for Au_{279} resemble what was observed for plasmonic gold nanoparticles.[16,17,24,25]

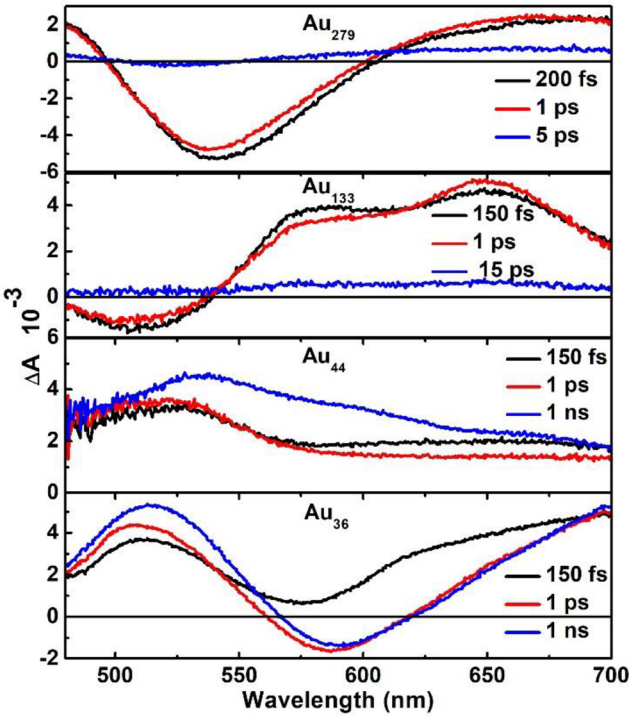

Figure 3. Excited-state absorption spectra at representative time delays for Au_{36}, Au_{44}, Au_{133}, and Au_{279} nanomolecules after excitation at 370 nm.

Although transient absorption spectra of Au_{279} have shown the signatures of the plasmonic bleach, it is important to prove if it indeed supports the plasmonic features. To examine the metallic character of Au_{279}, pump-power-dependent measurements were carried out for Au_{133} and Au_{279} NMs. The normalized transient decay traces of Au_{133} at 650 nm and Au_{279} at 540 nm are shown in parts A and B of Figure 4. It can be observed from the figure that no pump-power dependence was observed for Au_{133}, while small pump-power dependence can be seen for Au_{279}. The absence of pump-power dependence of transient decay traces of Au_{133} suggest the molecule-like nature, and a similar conclusion was reached in an earlier study on this nanomolecule.[22] The transient decay traces of both Au_{133} and Au_{279} at different pump powers were fitted to exponential decay functions, and the obtained lifetimes as a function of pump-power were shown in Figure 4C. It is evident that Au_{133} does not show any pump-power dependence while the decay lifetimes of Au_{279} increase with increase in pump-power consistent with a two-temperature model of electron−phonon relaxation.[17] Intense bleach with a maximum at 540 nm and *pump-power-dependent bleach recovery for Au_{279} prove the metallic character* of the nanocrystal and show that it can support plasmon absorption. A linear fit of the bleach recovery lifetimes of Au_{279} has yielded a slope of 0.91 ± 0.05 ps, which is close to what was reported for plasmonic gold clusters.[17] The transient absorption results conclusively show that Au_{279} supports

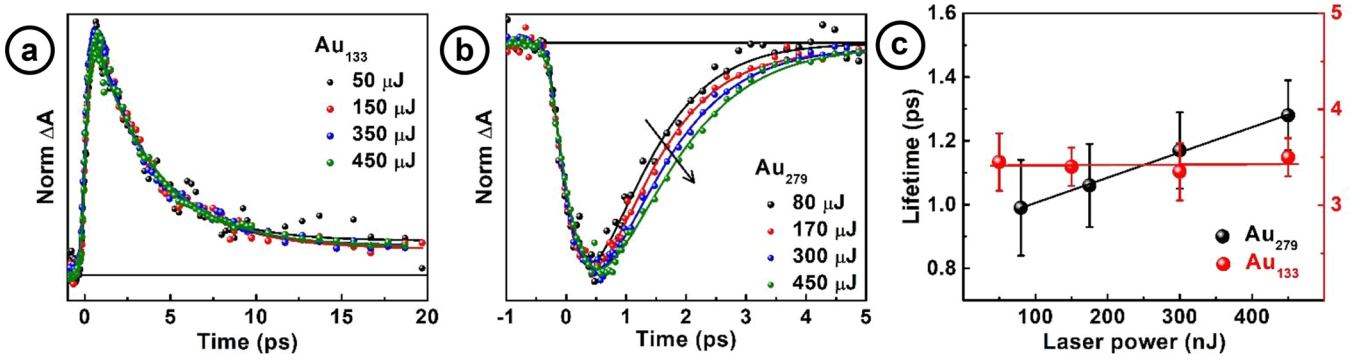

Figure 4. Pump-power-dependent transient decay traces of (a) Au_{133} monitored at 650 nm and (b) Au_{279} monitored at 540 nm. (c) Lifetimes as a function of laser power.

plasmonic transitions and the relaxation can be satisfactorily described by electron dynamics and a two-temperature model. This is by far the smallest ligand-protected gold nanocrystal that supports plasmonic absorption, the previous one being Au_{329}.[10,51] Optical gap, electrochemical gap, and electronically excited-state lifetimes of aromatic TBBT-protected AuNMs decrease with increase in size (see the Supporting Information for details).

In summary, the optical properties of F-279 nanocrystals were studied using combined steady-state and time-resolved absorption measurements and theoretical calculations. Experimental and calculated electronic absorption spectral features for F-279 suggest the presence of plasmonic absorption, whereas smaller nanomolecules show discrete electronic absorption features. Theoretical analysis and simulations confirm the birth of the plasmon resonance, with an additional contribution due to the resonance between excitations pertaining to the aromatic ligand and the Au−S shell. Transient absorption measurements for F-279 show a strong bleach and power-dependent bleach recovery kinetics similar to what was observed for gold clusters that can support plasmonic absorption.

AUTHOR INFORMATION

Corresponding Authors

*E-mail: alessandro.fortunelli@cnr.it.
*E-mail: rama.guda@wmich.edu.
*E-mail: amal@olemiss.edu.

ORCID

Mauro Stener: 0000-0003-3700-7903
Alessandro Fortunelli: 0000-0001-5337-4450
Guda Ramakrishna: 0000-0002-5288-8780
Amala Dass: 0000-0001-6942-5451

Notes

The authors declare no competing financial interest.

ACKNOWLEDGMENTS

NSF-CHE-1255519 supported the work performed by N.A.S. and A.D. Use of the Center for Nanoscale Materials, an Office of Science user facility, was supported by the U.S. Department of Energy, Office of science, Office of Basic Energy Sciences, under Contract No. DE-AC02-06CH11357. Support from CINECA supercomputing center within the ISCRA program is most gratefully acknowledged.

REFERENCES

(1) Lal, S.; Clare, S. E.; Halas, N. J. Nanoshell-Enabled Photothermal Cancer Therapy: Impending Clinical Impact. *Acc. Chem. Res.* **2008**, *41*, 1842−1851.

(2) Saha, S.; Xiong, X.; Chakraborty, P. K.; Shameer, K.; Arvizo, R. R.; Kudgus, R. A.; Dwivedi, S. K. D.; Hossen, M. N.; Gillies, E. M.; Robertson, J. D.; et al. Gold Nanoparticle Reprograms Pancreatic Tumor Microenvironment and Inhibits Tumor Growth. *ACS Nano* **2016**, *10*, 10636−10651.

(3) Linic, S.; Christopher, P.; Xin, H.; Marimuthu, A. Catalytic and Photocatalytic Transformations on Metal Nanoparticles with Targeted Geometric and Plasmonic Properties. *Acc. Chem. Res.* **2013**, *46*, 1890−1899.

(4) Atwater, H. A.; Polman, A. Plasmonics for Improved Photovoltaic Devices. *Nat. Mater.* **2010**, *9*, 205−213.

(5) Alvarez, M. M.; Khoury, J. T.; Schaaff, T. G.; Shafigullin, M. N.; Vezmar, I.; Whetten, R. L. Optical Absorption Spectra of Nanocrystal Gold Molecules. *J. Phys. Chem. B* **1997**, *101*, 3706−3712.

(6) Schaaff, T. G.; Shafigullin, M. N.; Khoury, J. T.; Vezmar, I.; Whetten, R. L.; Cullen, W. G.; First, P. N.; Gutierrez-Wing, C.; Ascensio, J.; Jose-Yacaman, M. J. Isolation of Smaller Nanocrystal Au Molecules: Robust Quantum Effects in Optical Spectra. *J. Phys. Chem. B* **1997**, *101*, 7885−7891.

(7) Ong, Q.; Luo, Z.; Stellacci, F. Characterization of Ligand Shell for Mixed-Ligand Coated Gold Nanoparticles. *Acc. Chem. Res.* **2017**, *50*, 1911−1919.

(8) Kelly, K. L.; Coronado, E. A.; Zhao, L. L.; Schatz, G. C. The Optical Properties of Metal Nanoparticles: The Influence of Size, Shape, and Dielectric Environment. *J. Phys. Chem. B* **2003**, *107*, 668−677.

(9) Cunningham, A.; Mühlig, S.; Rockstuhl, C.; Bürgi, T. Coupling of Plasmon Resonances in Tunable Layered Arrays of Gold Nanoparticles. *J. Phys. Chem. C* **2011**, *115*, 8955−8960.

(10) Dass, A. Faradaurate Nanomolecules: A Superstable Plasmonic 76.3 kDa Cluster. *J. Am. Chem. Soc.* **2011**, *133*, 19259−19261.

(11) Kumara, C.; Zuo, X.; Cullen, D. A.; Dass, A. Faradaurate-940: Synthesis, Mass Spectrometry, Electron Microscopy, High-Energy X-ray Diffraction, and X-ray Scattering Study of $Au_{\sim 940\pm 20}(SR)_{\sim 160\pm 4}$ Nanocrystals. *ACS Nano* **2014**, *8*, 6431−6439.

(12) Kumara, C.; Zuo, X.; Ilavsky, J.; Chapman, K. W.; Cullen, D. A.; Dass, A. Super-Stable, Highly Monodisperse Plasmonic Faradaurate-500 Nanocrystals with 500 Gold Atoms: $Au_{\sim 500}(SR)_{\sim 120}$. *J. Am. Chem. Soc.* **2014**, *136*, 7410−7417.

(13) Kumara, C.; Zuo, X.; Cullen, D. A.; Dass, A. $Au_{329-x}Ag_x(SR)_{84}$ Nanomolecules: Plasmonic Alloy Faradaurate-329. *J. Phys. Chem. Lett.* **2015**, *6*, 3320−3326.

(14) Malola, S.; Lehtovaara, L.; Enkovaara, J.; Häkkinen, H. Birth of the Localized Surface Plasmon Resonance in Monolayer-Protected Gold Nanoclusters. *ACS Nano* **2013**, *7*, 10263−10270.

(15) Negishi, Y.; Nakazaki, T.; Malola, S.; Takano, S.; Niihori, Y.; Kurashige, W.; Yamazoe, S.; Tsukuda, T.; Häkkinen, H. A Critical Size for Emergence of Nonbulk Electronic and Geometric Structures in Dodecanethiolate-Protected Au Clusters. *J. Am. Chem. Soc.* **2015**, *137*, 1206−1212.

(16) Link, S.; El-Sayed, M. A. Optical Properties and Ultrafast Dynamics of Metallic Nanocrystals. *Annu. Rev. Phys. Chem.* **2003**, *54*, 331−366.

(17) Hartland, G. V. Optical Studies of Dynamics in Noble Metal Nanostructures. *Chem. Rev.* **2011**, *111*, 3858−3887.

(18) Ramakrishna, G.; Varnavski, O.; Kim, J.; Lee, D.; Goodson, T. Quantum-Sized Gold Clusters as Efficient Two-Photon Absorbers. *J. Am. Chem. Soc.* **2008**, *130*, 5032−5033.

(19) Miller, S. A.; Womick, J. M.; Parker, J. F.; Murray, R. W.; Moran, A. M. Femtosecond Relaxation Dynamics of $Au_{25}L_{18}^-$ Monolayer-Protected Clusters. *J. Phys. Chem. C* **2009**, *113*, 9440−9444.

(20) Varnavski, O.; Ramakrishna, G.; Kim, J.; Lee, D.; Goodson, T. Critical Size for the Observation of Quantum Confinement in Optically Excited Gold Clusters. *J. Am. Chem. Soc.* **2010**, *132*, 16−17.

(21) Yi, C.; Tofanelli, M. A.; Ackerson, C. J.; Knappenberger, K. L. Optical Properties and Electronic Energy Relaxation of Metallic $Au_{144}(SR)_{60}$ Nanoclusters. *J. Am. Chem. Soc.* **2013**, *135*, 18222−18228.

(22) Zeng, C.; Chen, Y.; Kirschbaum, K.; Appavoo, K.; Sfeir, M. Y.; Jin, R. Structural Patterns at All Scales in a Nonmetallic Chiral $Au_{133}(SR)_{52}$ Nanoparticle. *Sci. Adv.* **2015**, *1*, e1500045.

(23) Thanthirige, V. D.; Kim, M.; Choi, W.; Kwak, K.; Lee, D.; Ramakrishna, G. Temperature-Dependent Absorption and Ultrafast Exciton Relaxation Dynamics in $MAu_{24}(SR)_{18}$ Clusters (M = Pt, Hg):

Role of the Central Metal Atom. *J. Phys. Chem. C* **2016**, *120*, 23180−23188.
(24) Zhou, M.; Zeng, C.; Chen, Y.; Zhao, S.; Sfeir, M. Y.; Zhu, M.; Jin, R. Evolution from the Plasmon to Exciton State in Ligand-Protected Atomically Precise Gold Nanoparticles. *Nat. Commun.* **2016**, *7*, 13240.
(25) Kwak, K.; Thanthirige, V. D.; Pyo, K.; Lee, D.; Ramakrishna, G. Energy Gap Law for Exciton Dynamics in Gold Cluster Molecules. *J. Phys. Chem. Lett.* **2017**, *8*, 4898−4905.
(26) Faraday, M. The Bakerian Lecture: Experimental Relations of Gold (and Other Metals) to Light. *Philos. Trans. R. Soc. London* **1857**, *147*, 145−181.
(27) Morton, S. M.; Silverstein, D. W.; Jensen, L. Theoretical Studies of Plasmonics using Electronic Structure Methods. *Chem. Rev.* **2011**, *111*, 3962−3994.
(28) Li, H.; Li, L.; Pedersen, A.; Gao, Y.; Khetrapal, N.; Jónsson, H.; Zeng, X. C. Magic-Number Gold Nanoclusters with Diameters from 1 to 3.5 nm: Relative Stability and Catalytic Activity for CO Oxidation. *Nano Lett.* **2015**, *15*, 682−688.
(29) Jiang, D.-e.; Tiago, M. L.; Luo, W.; Dai, S. The "Staple" Motif: A Key to Stability of Thiolate-Protected Gold Nanoclusters. *J. Am. Chem. Soc.* **2008**, *130*, 2777−2779.
(30) Desireddy, A.; Kumar, S.; Guo, J.; Bolan, M. D.; Griffith, W. P.; Bigioni, T. P. Temporal Stability of Magic-Number Metal Clusters: Beyond the Shell Closing Model. *Nanoscale* **2013**, *5*, 2036−2044.
(31) Fernando, A.; Weerawardene, K. L. D. M.; Karimova, N. V.; Aikens, C. M. Quantum Mechanical Studies of Large Metal, Metal Oxide, and Metal Chalcogenide Nanoparticles and Clusters. *Chem. Rev.* **2015**, *115*, 6112−6216.
(32) Baletto, F.; Ferrando, R. Structural Properties of Nanoclusters: Energetic, Thermodynamic, and Kinetic Effects. *Rev. Mod. Phys.* **2005**, *77*, 371−423.
(33) Barnard, A. S.; Curtiss, L. A. Predicting the Shape and Structure of Face-Centered Cubic Gold Nanocrystals Smaller than 3 nm. *ChemPhysChem* **2006**, *7*, 1544−1553.
(34) Barnard, A. S.; Lin, X. M.; Curtiss, L. A. Equilibrium Morphology of Face-Centered Cubic Gold Nanoparticles > 3 nm and the Shape Changes Induced by Temperature. *J. Phys. Chem. B* **2005**, *109*, 24465−24472.
(35) de Heer, W. A. The Physics of Simple Metal Clusters: Experimental Aspects and Simple Models. *Rev. Mod. Phys.* **1993**, *65*, 611−676.
(36) Heaven, M. W.; Dass, A.; White, P. S.; Holt, K. M.; Murray, R. W. Crystal Structure of the Gold Nanoparticle $[N(C_8H_{17})_4][Au_{25}(SCH_2CH_2Ph)_{18}]$. *J. Am. Chem. Soc.* **2008**, *130*, 3754−3755.
(37) Zhu, M.; Aikens, C. M.; Hollander, F. J.; Schatz, G. C.; Jin, R. Correlating the Crystal Structure of A Thiol-Protected Au_{25} Cluster and Optical Properties. *J. Am. Chem. Soc.* **2008**, *130*, 5883−5885.
(38) Qian, H.; Eckenhoff, W. T.; Zhu, Y.; Pintauer, T.; Jin, R. Total Structure Determination of Thiolate-Protected Au_{38} Nanoparticles. *J. Am. Chem. Soc.* **2010**, *132*, 8280−8281.
(39) Antonello, S.; Dainese, T.; Pan, F.; Rissanen, K.; Maran, F. Electrocrystallization of Monolayer-Protected Gold Clusters: Opening the Door to Quality, Quantity, and New Structures. *J. Am. Chem. Soc.* **2017**, *139*, 4168−4174.
(40) Dass, A.; Theivendran, S.; Nimmala, P. R.; Kumara, C.; Jupally, V. R.; Fortunelli, A.; Sementa, L.; Barcaro, G.; Zuo, X.; Noll, B. C. $Au_{133}(SPh\text{-}tBu)_{52}$ Nanomolecules: X-ray Crystallography, Optical, Electrochemical, and Theoretical Analysis. *J. Am. Chem. Soc.* **2015**, *137*, 4610−4613.
(41) Sakthivel, N. A.; Theivendran, S.; Ganeshraj, V.; Oliver, A. G.; Dass, A. Crystal Structure of Faradaurate-279: $Au_{279}(SPh\text{-}tBu)_{84}$ Plasmonic Nanocrystal Molecules. *J. Am. Chem. Soc.* **2017**, *139*, 15450−15459.
(42) Zeng, C.; Chen, Y.; Iida, K.; Nobusada, K.; Kirschbaum, K.; Lambright, K. J.; Jin, R. Gold Quantum Boxes: On the Periodicities and the Quantum Confinement in the Au_{28}, Au_{36}, Au_{44}, and Au_{52} Magic Series. *J. Am. Chem. Soc.* **2016**, *138*, 3950−3953.
(43) Zeng, C.; Qian, H.; Li, T.; Li, G.; Rosi, N. L.; Yoon, B.; Barnett, R. N.; Whetten, R. L.; Landman, U.; Jin, R. Total Structure and Electronic Properties of the Gold Nanocrystal $Au_{36}(SR)_{24}$. *Angew. Chem., Int. Ed.* **2012**, *51*, 13114−13118.
(44) Liao, L.; Chen, J.; Wang, C.; Zhuang, S.; Yan, N.; Yao, C.; Xia, N.; Li, L.; Bao, X.; Wu, Z. Transition-Sized Au_{92} Nanoparticle Bridging Non-FCC-Structured Gold Nanoclusters and FCC-Structured Gold Nanocrystals. *Chem. Commun.* **2016**, *52*, 12036−12039.
(45) Zeng, C.; Liu, C.; Chen, Y.; Rosi, N. L.; Jin, R. Atomic Structure of Self-Assembled Monolayer of Thiolates on a Tetragonal Au_{92} Nanocrystal. *J. Am. Chem. Soc.* **2016**, *138*, 8710−8713.
(46) Zeng, C.; Chen, Y.; Liu, C.; Nobusada, K.; Rosi, N. L.; Jin, R. Gold Tetrahedra Coil Up: Kekulé-Like and Double Helical Superstructures. *Sci. Adv.* **2015**, *1*, e1500425.
(47) Zeng, C.; Li, T.; Das, A.; Rosi, N. L.; Jin, R. Chiral Structure of Thiolate-Protected 28-Gold-Atom Nanocluster Determined by X-ray Crystallography. *J. Am. Chem. Soc.* **2013**, *135*, 10011−10013.
(48) Zhou, M.; Zeng, C.; Sfeir, M. Y.; Cotlet, M.; Iida, K.; Nobusada, K.; Jin, R. Evolution of Excited-State Dynamics in Periodic Au_{28}, Au_{36}, Au_{44}, and Au_{52} Nanoclusters. *J. Phys. Chem. Lett.* **2017**, *8*, 4023−4030.
(49) Zeng, C.; Chen, Y.; Kirschbaum, K.; Lambright, K. J.; Jin, R. Emergence of Hierarchical Structural Complexities in Nanoparticles and their Assembly. *Science* **2016**, *354*, 1580−1584.
(50) Zhou, M.; Zeng, C.; Song, Y.; Padelford, J. W.; Wang, G.; Sfeir, M. Y.; Higaki, T.; Jin, R. On the Non-Metallicity of 2.2 nm $Au_{246}(SR)_{80}$ Nanoclusters. *Angew. Chem., Int. Ed.* **2017**, *56*, 16257−16261.
(51) Kumara, C.; Dass, A. $Au_{329}(SR)_{84}$ Nanomolecules: Compositional Assignment of the 76.3 kDa Plasmonic Faradaurates. *Anal. Chem.* **2014**, *86*, 4227−4232.
(52) Xu, W. W.; Gao, Y. Unraveling the Atomic Structures of the $Au_{68}(SR)_{34}$ Nanoparticles. *J. Phys. Chem. C* **2015**, *119*, 14224−14229.
(53) Rambukwella, M.; Burrage, S.; Neubrander, M.; Baseggio, O.; Aprà, E.; Stener, M.; Fortunelli, A.; Dass, A. $Au_{38}(SPh)_{24}$: Au_{38} Protected with Aromatic Thiolate Ligands. *J. Phys. Chem. Lett.* **2017**, *8*, 1530−1537.
(54) Barcaro, G.; Sementa, L.; Fortunelli, A.; Stener, M. Optical Properties of Silver Nanoshells from Time-Dependent Density Functional Theory Calculations. *J. Phys. Chem. C* **2014**, *118*, 12450−12458.
(55) Barcaro, G.; Broyer, M.; Durante, N.; Fortunelli, A.; Stener, M. Alloying Effects on the Optical Properties of Ag−Au Nanoclusters from TDDFT Calculations. *J. Phys. Chem. C* **2011**, *115*, 24085−24091.
(56) Sementa, L.; Barcaro, G.; Dass, A.; Stener, M.; Fortunelli, A. Designing Ligand-Enhanced Optical Absorption of Thiolated Gold Nanoclusters. *Chem. Commun.* **2015**, *51*, 7935−7938.
(57) Van Voorhis, T.; Scuseria, G. E. A Novel Form for the Exchange-Correlation Energy Functional. *J. Chem. Phys.* **1998**, *109*, 400−410.
(58) Van Voorhis, T.; Scuseria, G. E. Erratum: "A Novel Form for The Exchange-Correlation Energy Functional" [J. Chem. Phys. 109, 400 (1998)]. *J. Chem. Phys.* **2008**, *129*, 219901.
(59) Nazarov, V. U.; Vignale, G. Optics of Semiconductors from Meta-Generalized-Gradient-Approximation-Based Time-Dependent Density-Functional Theory. *Phys. Rev. Lett.* **2011**, *107*, 216402.